



## Resonance and chaotic trajectories in magnetic field reversed configuration

A.S. Landsman <sup>a,\*</sup>, S.A. Cohen <sup>a</sup>, M. Edelman <sup>b</sup>, G.M. Zaslavsky <sup>b</sup>

<sup>a</sup> Princeton Plasma Physics Laboratory, P.O. Box 451, Princeton, NJ 08543, USA

<sup>b</sup> Courant Institute, 4 Washington Place, New York, NY 10003, USA

Received 6 January 2004; received in revised form 9 January 2004; accepted 9 January 2004

### Abstract

The nonlinear dynamics of a single ion in a field reversed configuration (FRC) were investigated. FRC is a toroidal fusion device which uses a specific type of magnetic field to confine ions. As a result of angular invariance, the full three-dimensional Hamiltonian system can be expressed as two coupled, highly nonlinear oscillators. Due to the high nonlinearity in the equations of motion, the behavior of the system is extremely complex, showing different regimes, depending on the values of the conserved canonical angular momentum and the geometry of the fusion vessel. Perturbation theory and averaging were used to derive an integrable Hamiltonian and frequencies of the two degrees of freedom. The derived equations were then used to find resonances and compare to Poincaré surface-of-section plots. A regime was found where the nonlinear resonances were clearly separated by KAM curves. The structure of the observed island chains was explained. The condition for the destruction of KAM curves and the onset of strong chaos was derived, using Chirikov island overlap criterion, and shown qualitatively to depend both on the canonical angular momentum and geometry of the device. After a brief discussion of the adiabatic regime, the paper goes on to explore the degenerate regime that sets in at higher values of angular momenta. In this regime, the unperturbed Hamiltonian can be approximated as two uncoupled linear oscillators. In this case, the system is near-integrable, except in cases of a universal resonance, which results in large island structures, due to the smallness of nonlinear terms, which bound the resonance. The linear force constants, dominant in this regime, were derived and the geometry for a large one-to-one resonance identified. The above analysis showed good agreement with numerical simulations and was able to explain characteristic features of the dynamics.

© 2003 Elsevier B.V. All rights reserved.

\* Corresponding author. Address: Plasma Physics, Princeton University, 235 Thunder Circle, Bensalem 19020, USA. Tel.: +1-215-702-1479/+1-609-243-2856; fax: +1-609-243-3185.

E-mail address: [landsman@princeton.edu](mailto:landsman@princeton.edu) (A.S. Landsman).

*PACS:* 52.55.Hc; 05.45.Pq; 05.45.Ac; 52.65.Cc; 52.20.Dq; 52.55.Ez

*Keywords:* Chaotic trajectories; Nonlinear oscillators; Resonances; Magnetic confinement

## 1. Introduction

The field-reversed configuration (FRC), see Fig. 1, is a toroidal-shaped magnetic-field geometry that appears well suited for confining plasmas for the purpose of the controlled, safe, steady-state production of fusion energy [1,2]. A primary characteristic that distinguishes the FRC from most other toroidal fusion devices is that it has no toroidal magnetic field. Thus charged-particle motion in FRCs cannot be approximated as being guided along magnetic field lines. For most fusion reactors, such as the tokamak, the magnetohydrodynamic (MHD) theory [3] has been used successfully to investigate the physics at fusion-relevant regimes. For the FRC, however it is well known [4,5] that in the fusion-relevant regime the single-particle Hamiltonian approach presents a powerful, applicable method to understand the qualitative features of ion dynamics.

The single ion dynamics inside the FRC have equations identical to those of two strongly coupled nonlinear oscillators. The strong nonlinearities make for a very interesting system with various regimes that depend on the values of the coupling constants. Thus both, a highly nonlinear regime with a set of island chains caused by nonlinear resonances and a linear regime with a single large universal resonance caused by the intrinsic degeneracy can be observed.

Stochastic dynamics and resonances in nonlinear oscillators have been extensively studied in various cases of theoretical and practical interest [6–12]. The present paper is the first detailed study of the model of coupled resonances that are related to FRC. Using averaging methods and perturbation theory, we investigate particle dynamics in the FRC under the variation of two control parameters: geometric factor  $\beta$ , which is inverse elongation (or aspect ratio of the FRC in

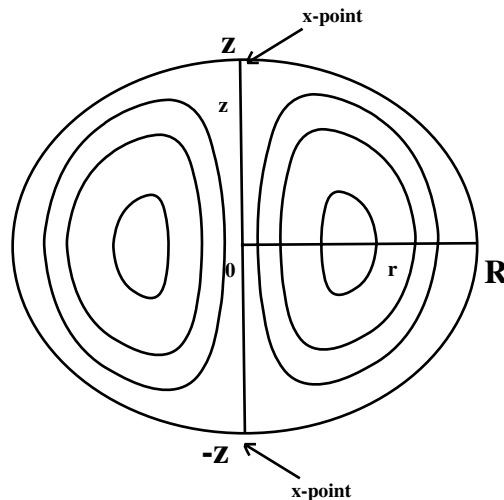


Fig. 1. Geometry of the field-reversed configuration of magnetic field. Lines correspond to the cross-section of surfaces of constant magnetic flux,  $\Phi$  (see Eq. (2)).

Fig. 1) and dimensionless azimuthal angular momentum,  $P$ , that is conserved due to the azimuthal symmetry of the field. It is found that variation of  $\beta$  and  $P$  significantly affect the resonance structure and level of stochasticity.

The paper is organized as follows: In Section 2 the problem is set up and a two-dimensional Hamiltonian is derived using conservation of azimuthal angular momentum,  $P$ . The derived Hamiltonian is then used to discuss possible types of particle orbits that can occur in the FRC for  $P > 0$  ions. In Section 3, the impact of  $P$  and elongation on resonance structure and stochasticity is studied using the Hamiltonian derived in Section 2. First, the unperturbed Hamiltonian  $H_0$  is derived using averaging methods. It is found that for certain range of values of elongation and azimuthal angular momenta, the unperturbed Hamiltonian is sufficiently nonlinear and the perturbation sufficiently small, that KAM theory applies and a resonant island structure bounded by KAM curves is obtained. The paper then goes on to discuss the breakdown of KAM theory with variation of parameters and the onset of strong chaos. The adiabatic regime, occurring in the large elongation (small  $\beta$ ) limit, where a significant frequency separation occurs between the two degrees of freedom is also discussed. In Section 4, we turn to the near-integrable case that occurs in the limit of higher azimuthal angular momenta. It is shown that in this limit, the unperturbed Hamiltonian has the form of two uncoupled harmonic oscillators, so that action-angle variables of a simple harmonic oscillator can be used in the Hamiltonian expansion. After explaining why the system is near-integrable at higher azimuthal angular momenta for elongation close to or less than one, we turn to the case of a large one-to-one universal resonance. It is shown that this large resonance is a consequence of intrinsic degeneracy, while the set of smaller resonances occurring at smaller azimuthal angular momenta values is a result of accidental degeneracy.

## 2. Equations of motion and orbit types

### 2.1. Basic equations of motion

The Hamiltonian for a nonrelativistic particle of charge  $q$  in a magnetic field is given by [13]:

$$H = \frac{1}{2} \left[ (p_r - qA_r)^2 + (p_z - qA_z)^2 + \left( \frac{p_\phi}{r} - qA_\phi \right)^2 \right] \quad (1)$$

where  $A_{r,z,\phi}$  are the components of the vector potential and  $p_{r,z,\phi}$  are the canonical angular momenta. As a representative FRC system, a Solov'ev model [14] is used in which the plasma pressure has a linear dependence on magnetic flux  $\Phi$ :

$$\Phi = rA_\phi \quad (2)$$

In this model, the magnetic flux is described by [15]:

$$\Phi = R^2 B_a \frac{r^2}{2R^2} \left( 1 - \frac{r^2}{R^2} - \frac{\beta^2 z^2}{R^2} \right) \quad (3)$$

where  $B_a$  is the amplitude of the magnetic field at the center of the device at  $r = z = 0$ ,  $R$  is the radius of the separatrix on the midplane at  $z = 0$ , and  $2Z$  is the distance between  $X$ -points along the  $z$ -axis:  $\beta = R/Z$ . Eq. (3) shows a pressure profile that falls to zero at the boundary of the device

where  $\Phi = 0$ . From Eqs. (2) and (3), we can obtain a vector potential,  $A_\phi$ . Since the full vector potential of the FRC has only a  $\phi$  component, we get the following expression for the vector potential:

$$\vec{A} = A_\phi \hat{\phi} = B_a \frac{r}{2} \left( 1 - \frac{r^2}{R^2} - \frac{\beta^2 z^2}{R^2} \right) \hat{\phi} \quad (4)$$

where  $\hat{\phi}$  is a unit vector in the azimuthal direction. Substituting the vector potential from Eq. (4) into Eq. (1), the Hamiltonian becomes:

$$H = \frac{1}{2m} \left[ p_r^2 + p_z^2 + \left( \frac{p_\phi}{r} - qA_\phi \right)^2 \right] \quad (5)$$

where  $p_\phi$  is the conserved canonical azimuthal angular momentum. Substitution of  $A_\phi$  from Eq. (4) into Eq. (5) gives

$$H = \frac{1}{2m} \left\{ p_r^2 + p_z^2 + \left[ \frac{p_\phi}{r} - br \left( 1 - \frac{r^2}{R^2} - \frac{\beta^2 z^2}{R^2} \right) \right]^2 \right\} \quad (6)$$

where  $b = qB_a/2$ . The azimuthal angular momentum  $p_\phi$  is conserved since there is no angular dependence in the Hamiltonian. The Hamiltonian above describes a two degree of freedom time-independent system. After scaling  $r/R \rightarrow r$ ,  $z/R \rightarrow z$ ,  $p_r/bR \rightarrow p_r$ ,  $p_z/bR \rightarrow p_z$  and  $(m/b^2R^2)H \rightarrow H$ , the dimensionless Hamiltonian becomes:

$$H = \frac{1}{2} \left\{ p_r^2 + p_z^2 + \left[ \frac{P}{r} - r(1 - r^2 - \beta^2 z^2) \right]^2 \right\} \quad (7)$$

where  $P = p_\phi/bR^2$ . The last term is a two-dimensional potential  $V(r, z)$ :

$$V(r, z) = \frac{1}{2} \left[ \frac{P}{r} - r(1 - r^2 - \beta^2 z^2) \right]^2 \quad (8)$$

After applying Hamiltonian equations of motion

$$\dot{q}_i = \frac{\partial H}{\partial p_i}; \quad \dot{p}_i = -\frac{\partial H}{\partial q_i} \quad (9)$$

where  $q_i$  and  $p_i$  are the coordinate and momentum variables, we get

$$\ddot{r} + r(1 + 2P) - \frac{P^2}{r^3} - 4r^3 + 3r^5 + \beta^2 z^2(4r^3 - 2r + \beta^2 z^2 r) = 0 \quad (10)$$

$$\ddot{z} + 2\beta^2 z [P - r^2(1 - r^2 - \beta^2 z^2)] = 0 \quad (11)$$

Note that the  $\beta$  variable cannot be scaled away since it appears in Eq. (11) as a  $\beta^2 z$  term, and effects the time scale of  $z$  motion relative to  $r$  motion.

From Eq. (11), the force along  $z$  is zero when  $z = 0$ . Given the initial condition  $z = p_z = 0$ , the ion will stay confined to the  $z = 0$  plane, where the motion is one-dimensional and therefore integrable. The integrable motion in the  $z = 0$  subspace is briefly described in the following section.

### 2.2. Types of orbits

The possible types of orbits in the  $z = 0$  subspace have been previously discussed [16,17]. For positive values of  $P$ , there are two possible shapes for a potential well  $V$  as a function of  $r$ . It is either a double well with minima touching zero or a single raised well. Fig. 2 shows different shapes of  $V$ , for various values of  $P$  in the  $z = 0$  subplane. Higher values of  $P$  result in a shallower potential, see also Eq. (7), until there is a transition to a single raised potential at a critical value of  $P_c = 1/4$ . Fig. 3 shows cross-sections of the potential as a function of  $r$  for different values of  $z$ . It can be seen that the double potential becomes shallower as  $|z|$  increases, eventually turning into a single raised potential. For values of  $P$  above the critical threshold, the entire potential well becomes further raised as the ion travels towards higher absolute values of  $z$ .

To explain the different types of orbits observed, it is worth noting that the potential  $V$  in the reduced two-dimensional system is actually the kinetic energy in the  $\phi$  direction in the full three-dimensional system. This is due to the fact that only magnetic fields are present, which exert a Lorentz force perpendicular to the direction of motion:  $\vec{F} = q\vec{v} \times \vec{B}$ , therefore the total kinetic energy is conserved. It follows that

$$H = \frac{1}{2m} [p_r^2 + p_z^2 + (mr\dot{\phi})^2] \tag{12}$$

Comparing Eq. (12) with Eq. (6), it is clear that the last terms are equal. Since  $r^2\dot{\phi}^2$  is proportional to  $V$ , it follows that  $\dot{\phi}$  changes sign whenever the potential  $V$  touches zero (except at the transition to a single raised potential), therefore the ion reverses its angular direction of motion. Based on the types of potential described above, we can now explain the three possible types of orbits observed in the FRC for positive values of  $P$ , see Fig. 4. First, there are cyclotron orbits which correspond to oscillations in one of the two wells of the double potential in the radial direction.

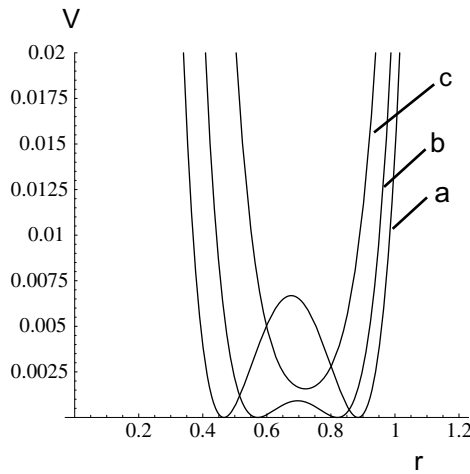


Fig. 2. Possible shapes of potential in the  $z = 0$  subplane: (a)  $P = 0.17$ ; (b)  $P = 0.22$ ; and (c)  $P = 0.29$ . Below  $P = P_c = 1/4$ , the potential has a shape of a double well, and above a raised single well. The top of the potential barrier occurs at  $r_h(P, z)$ , see Eq. (26).

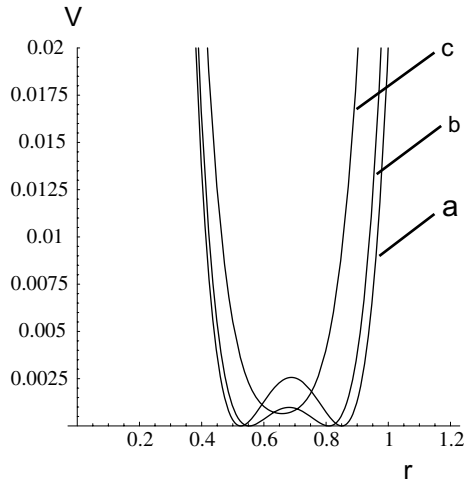


Fig. 3. Cross-sections of the potential  $V$  for  $P = 0.2$ : (a)  $z = 0$ ; (b)  $z = 0.2$ ; and (c)  $z = 0.3$ . For positive  $P$  ions, the barrier in the double potential drops as  $|z|$  increases, until it turns into a single raised potential. The barrier between the two zeros in the potential is the  $\dot{\phi} < 0$  part of the orbit, while  $\dot{\phi} > 0$  to the left and to the right of the potential barrier.

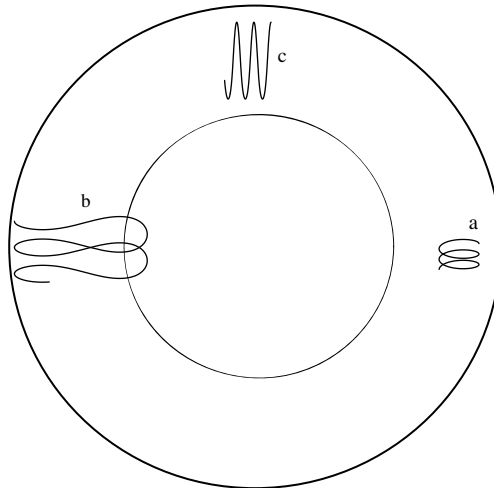


Fig. 4. Possible types of particle orbits for  $P > 0$ . Orbits are taken in the  $z = 0$  invariant subspace. The outer circle indicates the zero in magnetic flux,  $\Phi$  (also the boundary of the vessel). The inner circle is at the inner minima of the double potential for  $P = 0.2$ . (a) Cyclotron orbit: ion oscillates in the outer portion of a double well,  $P = 0.2$ ; (b) figure-8 orbit: ion oscillates over the entire double well,  $P = 0.2$ ; (c) betatron orbits: oscillations in a raised potential,  $P = 0.35$ .

They are unstable to displacement from the mid-plane and therefore tend to travel to higher absolute values of  $z$ . The second type of orbits are figure-8 orbits which oscillate over the entire double potential. Since the barrier dividing the two wells exerts a repelling force, as can be shown by plotting Eq. (11) as a function of  $r$  (keeping  $z$  constant), higher energy figure-8 orbits are stable

around  $z = 0$  while lower energy ones, which spend more of their time transversing the barrier are unstable around  $z = 0$ . All double potential wells become shallower as an ion moves towards higher values of  $|z|$ , so that all cyclotron orbits will eventually have enough energy to cross the barrier in the double potential (for some nonzero value of  $z$ ) and turn into figure-8 orbits, thus eventually feeling a restoring force towards  $z = 0$ . The third type of orbit is the betatron orbit, shown in Fig. 2c, which corresponds to oscillations in a raised potential. It is characterized by  $\dot{\phi} > 0$  at all times, which is explained by considering that the potential  $V$  never touches zero, and therefore  $\dot{\phi}$  never undergoes a sign change. Betatron orbits are stable to displacements from  $z = 0$ .

### 3. Resonances and chaos

#### 3.1. Averaged equations of motion

The Hamiltonian in Eq. (7) can be expanded as,

$$H = H_{r0}(p_r, r) + H_{z0}(p_z, z) + \epsilon H_1(r, z) \quad (13)$$

where  $H_0 = H_{r0}(p_r, r) + H_{z0}(p_z, z)$  is the uncoupled, integrable portion of the Hamiltonian, and  $\epsilon$  is the magnitude of the coupled terms. If  $H_1$  is normalized to the same magnitude as  $H_0$ ,  $\epsilon$  gives the degree of perturbation to the integrable portion of the Hamiltonian,  $H_0$ . The above Hamiltonian can be expressed in action-angle variables of the uncoupled Hamiltonian,  $H_0$ .

$$H = H_{r0}(J_{r0}) + H_{z0}(J_{z0}) + \epsilon H_1(\vec{J}_0, \vec{\theta}_0) \quad (14)$$

where  $\vec{J}_0 = (J_{r0}, J_{z0})$  and  $\vec{\theta}_0 = (\theta_{r0}, \theta_{z0})$  are the conjugate action-angle variables of  $H_0$ . Actions  $J_{r0}$  and  $J_{z0}$  are the areas enclosed by the unperturbed trajectory in phase-space,

$$J_{r0} = \frac{1}{2\pi} \oint p_r dr, \quad J_{z0} = \frac{1}{2\pi} \oint p_z dz \quad (15)$$

where the integrals are taken over one oscillation in their respective coordinates.  $H_{r0}$  and  $H_{z0}$  are used to evaluate  $p_r$  and  $p_z$ , respectively, used in Eq. (15). The equations of motion can be written as

$$\dot{J}_{r0} = -\epsilon \frac{\partial H_1}{\partial \theta_{r0}}; \quad \dot{J}_{z0} = -\epsilon \frac{\partial H_1}{\partial \theta_{z0}}; \quad \dot{\theta}_{r0} = \omega_{r0} = \frac{\partial H_{r0}}{\partial J_{r0}}; \quad \dot{\theta}_{z0} = \omega_{z0} = \frac{\partial H_{z0}}{\partial J_{z0}} \quad (16)$$

where  $\omega_{r0}$  and  $\omega_{z0}$  are the frequencies of the unperturbed Hamiltonian  $H_0$  and  $(\theta_{r0}, \theta_{z0})$  are defined using a generating function [6],

$$S = \sum_{q=r,z} \int_{q_0}^q p_q dq \quad (17)$$

where

$$\theta_{r0} = \frac{\partial S}{\partial J_{r0}}, \quad \theta_{z0} = \frac{\partial S}{\partial J_{z0}} \quad (18)$$

The perturbation term  $H_1$  can be expanded in terms of action-angle variables:

$$H_1 = \sum_{l,m=-\infty}^{\infty} H_{l,m}(\vec{J}_0) \exp(i\vec{n} \cdot \vec{\theta}_0) \quad (19)$$

where  $\vec{n} = (l, m)$  is an integer vector. In  $(r, z)$  variables  $H_1$  can be obtained from the Hamiltonian in Eq. (7),

$$\epsilon H_1 = -r^2 \beta^2 z^2 + r^4 \beta^2 z^2 + \frac{1}{2} r^2 \beta^4 z^4 \quad (20)$$

If the coupling is sufficiently small and there is sufficient nonlinearity, such that the conditions of KAM theory are satisfied, there exist a series of resonances bounded by KAM curves. The KAM curves are perturbed from the uncoupled Hamiltonian  $H_0$  and can be obtained using perturbation theory. Resonance occurs whenever

$$s\omega_{r0} - q\omega_{z0} = 0 \quad (21)$$

where  $s, q$  are integers and  $\omega_{r0}, \omega_{z0}$  are given by Eq. (16). When the condition given by Eq. (21) occurs, there are slowly varying terms in the exponent of the expansion of  $H_1$  in Eq. (19), leading to a significant perturbation in the Hamiltonian.

In the absence of resonances, the Hamiltonian given by Eq. (13) can be averaged along  $z$  and  $r$  to obtain averaged motion along  $r$  and  $z$ , respectively. This is equivalent to averaging Eq. (14) over  $\theta_{z0}$  to get the averaged  $r$  motion and over  $\theta_{r0}$  to get the averaged  $z$  motion, with  $H_1$  given by Eq. (19). All the angle dependent terms in  $H_1$  will average to zero, except for the resonant terms [7,10]. After averaging Eq. (13) over  $z$  and  $r$ , we obtain  $\overline{H}_r(r)$  and  $\overline{H}_z(z)$ , respectively, which represent averaged Hamiltonians for  $r$  and  $z$  motion,

$$\overline{H}_r(r) = H_{r0}(p_r, r) + \epsilon \langle H_1(r, z) \rangle_z \quad (22)$$

$$\overline{H}_z(z) = H_{z0}(p_z, z) + \epsilon \langle H_1(r, z) \rangle_r \quad (23)$$

Using these new Hamiltonians, and following the same procedure as before, one can obtain the new actions  $J_r$  and  $J_z$ , that would contain higher-order corrections to  $J_{r0}$  and  $J_{z0}$ . The frequencies  $\omega_r$  and  $\omega_z$  obtained using  $\overline{H}_r(J_r)$  and  $\overline{H}_z(J_z)$  can then be used to find the location of resonances, when

$$s\omega_r - q\omega_z = 0 \quad (24)$$

Here,  $(\omega_r, \omega_z)$  are corrections to  $(\omega_{r0}, \omega_{z0})$ . To find the averaged Hamiltonian along  $z$ , we need to substitute an approximate solution for the  $r$  motion into Eq. (7) The motion along  $r$  can be approximated as

$$r \approx r_h + A \cos(\omega_r t) \quad (25)$$

where  $r_h$  is the midpoint of oscillation. It is found by setting the derivative of the potential in Eq. (8) equal to zero and solving for  $r$ . Eq. (25) takes the first term in the Fourier expansion of the motion along  $r$ . For  $\beta^2 z^2 \ll 1$ ,  $r_h$  can be approximated as

$$r_h \approx (K_1 - K_2 \beta^2 z^2)^{1/2} \quad (26)$$

where

$$K_1 = \frac{1}{6}(1 + C_1); \quad K_2 = \frac{1}{6}(1 + 1/C_1); \quad C_1 = (1 + 12P)^{\frac{1}{2}} \quad (27)$$

Substituting Eq. (25) into Eq. (7), expanding and keeping only the highest order nonoscillatory terms, we get the averaged unperturbed Hamiltonian along  $z$ :

$$\overline{H}_z \approx \frac{1}{2}p_z^2 + \frac{1}{2}(D_z\beta^2z^2 + F_z\beta^4z^4) \quad (28)$$

where  $D_z$  is a function of  $P$  and  $A$ , with  $A$  given by Eq. (25). The value of  $F_z$  is not dependent on  $P$ , as can be easily confirmed by expanding the potential. It follows that the magnitude of the  $z^4$  term in Eq. (28) stays constant as  $P$  is increased. The quadratic term however, changes significantly as  $P$  is varied, which can be seen by expanding the potential given in Eq. (7).

To obtain  $H_{r0}$ , we follow a similar procedure as that used to obtain  $H_{z0}$  and approximate the motion along  $z$  as,

$$\beta z \approx B \cos(\omega_z t) \quad (29)$$

where  $B$  is the amplitude of oscillation along  $z$ .  $B < 1$  for ions confined inside the FRC. It is convenient to change variables to  $\Delta r = r - r_0$ , where  $r_0 = K_1^{1/2}$  (see Eq. (26)). Since this is a simple coordinate shift, the momentum,  $p_r$ , is not effected by the transformation. Substituting Eq. (29) into Eq. (7), we get, after expanding the  $P^2/r^2$  term in a series and dropping higher-order and oscillatory terms,

$$\overline{H}_r \approx \frac{1}{2}p_r^2 + \frac{1}{2}(D_r\Delta r^2 + M_r\Delta r^3 + F_r\Delta r^4) \quad (30)$$

The coefficients  $D_r$ ,  $M_r$ , and  $F_r$  are a function of azimuthal angular momentum  $P$ , and, in higher-order, depend on  $B$ , or the amplitude of oscillation along  $z$ . To lowest order (neglecting amplitude dependent terms), the coefficients in Eq. (30) can be expressed in terms of  $K_1$  and  $K_2$  (see Eq. (27)) which are functions of  $P$  only. Approximate expressions for  $F_r$  and  $F_z$  as functions of  $K_1$  and  $K_2$  will be given in the next section, where the contribution of these terms to nonlinear resonance is discussed. The above approximations fail for low amplitude cyclotron orbits whose motion cannot be expanded around  $r_0 = K_1^{1/2}$ . The measure of such orbits in phase-space decreases with increasing azimuthal angular momentum,  $P$ .

Eqs. (28) and (30) give approximate unperturbed averaged Hamiltonians for the  $z$  and  $r$  motion. From these equations, the actions  $J_z$  and  $J_r$  can be obtained using Eq. (15). These actions will be approximately conserved in the absence of resonances. Expressing  $\overline{H}_r$  and  $\overline{H}_z$  in terms of  $J_r$  and  $J_z$ , respectively, the frequencies of averaged  $r$  and  $z$  motion, given by Eq. (16), become

$$\omega_r = \frac{\partial \overline{H}_r}{\partial J_r}; \quad \omega_z = \frac{\partial \overline{H}_z}{\partial J_z} \quad (31)$$

In the next section, the approximate dependence of  $\overline{H}_r$  on  $J_r$  and  $\overline{H}_z$  on  $J_z$  is derived and the frequencies  $\omega_r, \omega_z$  obtained for the case of “intermediate” values of  $P$  where Eqs. (28) and (30) become further simplified.

3.2. Nonlinear resonances

The averaged Hamiltonians derived in the previous section can be used to find the location of nonlinear resonances. Fig. 5 shows the lowest-order values of the coefficients in Eqs. (28) and (30), as a function of  $P$  for the averaged  $r$  and  $z$  motion. The higher-order amplitude dependent terms are not included since they vary with different trajectories. It can be seen that all except the fourth power coefficients are zero around  $P \approx P_c$ . Amplitude dependent terms make a positive contribution, shifting the coefficient curves upward and causing them to intersect the  $P$ -axis at a lower values. Since  $P_c$  denotes the transition to betatron orbits and a typical FRC has a significant amount of figure-8 and cyclotron orbits, this range of  $P$  values can be considered as “intermediate”. Thus in this intermediate range, centered around  $P_i < P_c$ , the fourth power terms predominate for both  $r$  and  $z$  motion. For typical ion energies used in the numerical simulations, which allow the ion to explore most of the FRC while remaining inside it, this range is around

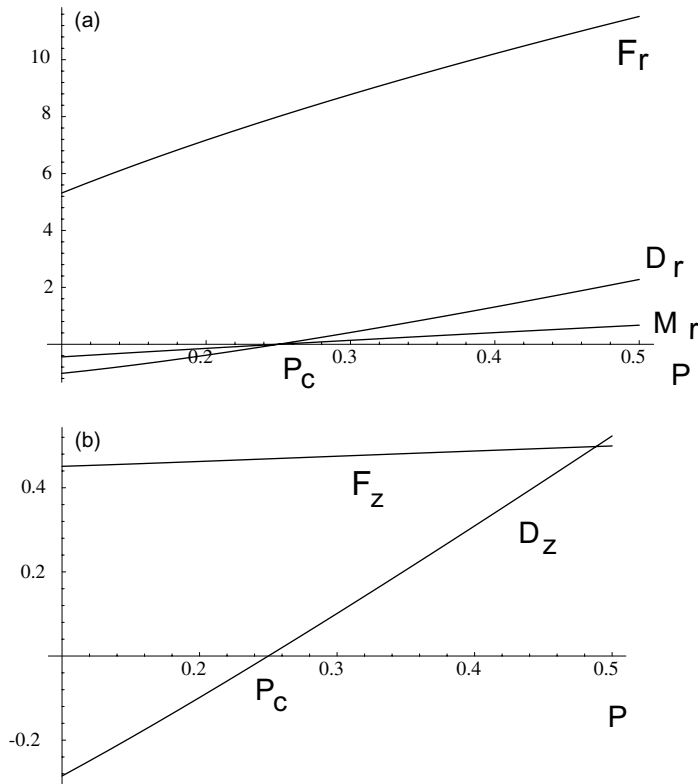


Fig. 5. Approximate coefficients for the averaged motion, neglecting amplitude contributions. (a)  $F_r$  is the coefficient for the fourth power term of  $\bar{H}_r$ .  $D_r$  and  $M_r$  are coefficients for the quadratic and third power terms, respectively. Although they seem to intersect the  $x$ -axis around  $P \approx P_c$ , amplitude dependent terms cause  $D_r$  and  $M_r$  to shift upwards, lowering the value of  $P$  at which these terms are negligible. (b)  $F_z$  is the coefficient for the fourth power term of  $\bar{H}_z$  and  $D_z$  is the coefficient for the quadratic term. Like in the above case, higher-order amplitude dependent terms cause  $D_z$  to shift upwards.

$(3/4)P_c < P < P_c$ . Approximating  $\bar{H}_r$  and  $\bar{H}_z$  in Eqs. (30) and (28) for intermediate values of  $P$ , we get

$$\bar{H}_r \approx \frac{1}{2}p_r^2 + \frac{1}{2}F_r \Delta r^4 \tag{32}$$

$$\bar{H}_z \approx \frac{1}{2}p_z^2 + \frac{1}{2}F_z \beta^4 z^4 \tag{33}$$

It will be shown later that variations in  $F_r$  and  $F_z$  have a weak effect on the unperturbed frequencies,  $\omega_r$  and  $\omega_z$ , respectively. It follows that higher-order terms can be dropped without having a significant effect on frequencies. After dropping higher-order amplitude dependent terms, the coefficients can be approximated as:

$$F_r \approx -2 + 15K_1 + \frac{4P}{K_1} + \frac{P^2}{K_1^3} \tag{34}$$

$$F_z \approx K_1 + 2K_2 - 4K_1K_2 - 2K_2^2 + 3K_1K_2^2 \tag{35}$$

For motion along  $z$ , the  $A^2$  amplitude terms (obtained by substituting Eq. (25) into the Hamiltonian) make a positive contribution to quadratic and fourth power terms, and thus contribute to stability around  $z = 0$ . It follows that oscillations that have higher energies along  $r$  are confined closer to the midplane [17,18]. Both  $K_1$  and  $K_2$  (see Eq. (27)) are less than one at intermediate values of  $P$ . Looking at Eqs. (34) and (35) or Fig. 5, it can be seen that  $F_r \gg \beta^4 F_z$ , except at “high” values of  $\beta$  (close to two), corresponding to oblate geometry. Comparing Eqs. (32) and (33), it can be seen that for the same amplitudes of oscillation, the frequency of motion along  $r$  will be significantly higher than along  $z$ . Keeping in mind that for these nonlinear oscillators, the frequencies of oscillation increases with amplitude, it becomes clear that the important primary nonlinear resonances (those that have the greatest island width and can therefore be easily observed) occur when  $\bar{H}_r \ll \bar{H}_z$ .

Using Eqs. (32) and (33), we can now derive primary nonlinear resonances defined as:

$$\omega_z/\omega_r = s/q \tag{36}$$

where  $s, q$  are integers and  $\omega_r, \omega_z$  are the unperturbed frequencies.

Eqs. (32) and (33) have a Hamiltonian of the form:

$$H = \frac{1}{2}p^2 + \frac{1}{2}Fq^4 = E \tag{37}$$

where  $F$  and  $E$  are constants. The action integral in this case is equal to:

$$J = \frac{2}{\pi} \int_0^{q_{\max}} (2E - Fq^4)^{1/2} dq \tag{38}$$

where  $q_{\max} = (2E/F)^{1/4}$ . Expanding the expression inside the integral using the formula

$$G(x_0 + \Delta x) = \sum_{n=0}^{\infty} G^n(x_0) \frac{(\Delta x)^n}{n!} \tag{39}$$

where  $G^n(x_0)$  signifies the  $n$ th derivative of the function, we get:

$$(2E - Fq^4)^{1/2} = \sqrt{2E} - \frac{(2E)^{-1/2}}{2} Fq^4 - \sum_{n=2}^{\infty} \frac{(2E)^{(1/2-n)}}{2^n} \frac{F^n q^{4n}}{n!} \prod_{j=1}^{n-1} (2j - 1) \quad (40)$$

Substituting Eq. (40) into the integral in Eq. (38), and integrating, we get an expression for  $J$

$$J = aE^{3/4}F^{-1/4} \quad (41)$$

where  $a$  is a constant

$$a = \frac{2^{7/4}}{\pi} \left[ 1 - \frac{\sqrt{2}}{5} - \sum_{n=2}^{\infty} \frac{1}{2^n n! (4n + 1)} \prod_{j=1}^{n-1} (2j - 1) \right] \quad (42)$$

rearranging Eq. (41) and using Eq. (37) to get an expression for the Hamiltonian  $H$  in terms of the conserved action variable  $J$ , we get:

$$H = a^{-4/3} F^{1/3} J^{4/3} \quad (43)$$

with  $a$  defined by Eq. (42). Applying Hamilton's equation  $\dot{\theta} = \omega = \partial H / \partial J$  to Eq. (43) and then substituting for  $J$  from Eq. (41), we get an expression for frequency as a function of energy.

$$\omega = \frac{4}{3a} (HF)^{1/4} \quad (44)$$

To find the averaged frequencies  $\omega_r$  and  $\omega_z$ ,  $F$  in Eq. (44) has to be replaced by  $F_r$  and  $\beta^4 F_z$ , respectively. Likewise,  $H$  should be replaced by  $\bar{H}_r$  and  $\bar{H}_z$  or  $H_r$  and  $H_z$  which are easily calculated from  $H$  at  $z = 0$ :

$$H_r = \frac{1}{2} p_r^2 + V(r, 0); \quad H_z = \frac{1}{2} p_z^2 \quad (45)$$

and are close to  $\bar{H}_r$  and  $\bar{H}_z$  near the elliptical center of the resonance (in accordance with Birckhoff theorem) [7]. Note from Eq. (44) that  $\omega$  is not sensitive to small variation in  $F$  and  $H$ , thus we were justified in dropping smaller order amplitude of oscillation dependent terms in the expressions for  $F_r$  and  $F_z$ .

From Eq. (44), we can now obtain a general criteria for nonlinear primary resonance that occurs at intermediate values of  $P$  where Eqs. (32) and (33) apply. Using the expression for frequency given by Eqs. (44) and (36)

$$\frac{\bar{H}_z F_z \beta^4}{\bar{H}_r F_r} = \left( \frac{s}{q} \right)^4 \quad (46)$$

The equation shows that small changes in  $s/q$  require large changes in  $\bar{H}_z / \bar{H}_r$ .

### 3.3. Location of resonances and the effect of geometry

The amount of stochasticity and location of resonances is strongly affected by geometry of the fusion vessel. Eq. (46) can be used to compute the location of various nonlinear resonances and explore the effect of changes in geometry (variation in  $\beta$ ). For example, taking  $\beta = 1$  as a con-

venient starting point, and using Eq. (46), there is a one-to-one primary resonance around  $H_z = (F_r/F_z)H_r$ .

To find the location  $r$  of this resonance for the initial condition  $p_r = z = 0$ , we need to use a “high” value of total energy  $H$ , which allows the ion trajectory access to most of the vessel, while not going far outside the boundary set by  $\Phi = 0$  so that the conditions under which Eq. (33) was derived are satisfied (see for example Fig. 6). Starting from initial conditions  $z = p_r = 0$  and using Eq. (45), we get:  $H_z = \frac{1}{2}p_z^2$ ,  $H_r = V(r, 0)$ , when  $t = 0$ . Applying the conditions  $H_r + H_z = H$  and  $H_z = (F_r/F_z)H_r$  to express  $H_r$  in terms of the total energy, the location,  $r$ , of a one-to-one resonance at  $z = p_r = 0$  is found by solving the following equation for  $r$ .

$$HF_z/(F_r + \beta^4 F_z) = V(r, 0) \tag{47}$$

Fig. 7 shows one-to-one resonances close to  $r \approx 0.58, 0.95$ , values which agrees well with the ones obtained by solving the above equation. Lesser values of total energy  $H$  shift the location of this resonance inward towards lower values of  $r \approx r_h$ , while higher  $H$  shift the resonance outward. This is explained by using Eq. (46) where an increase in  $H$  would lead to proportionate increases in  $H_z$  and  $H_r$  (keeping everything else constant) and therefore an outward shift in the location of a one-to-one resonance towards higher values of  $V(r, 0)$ .

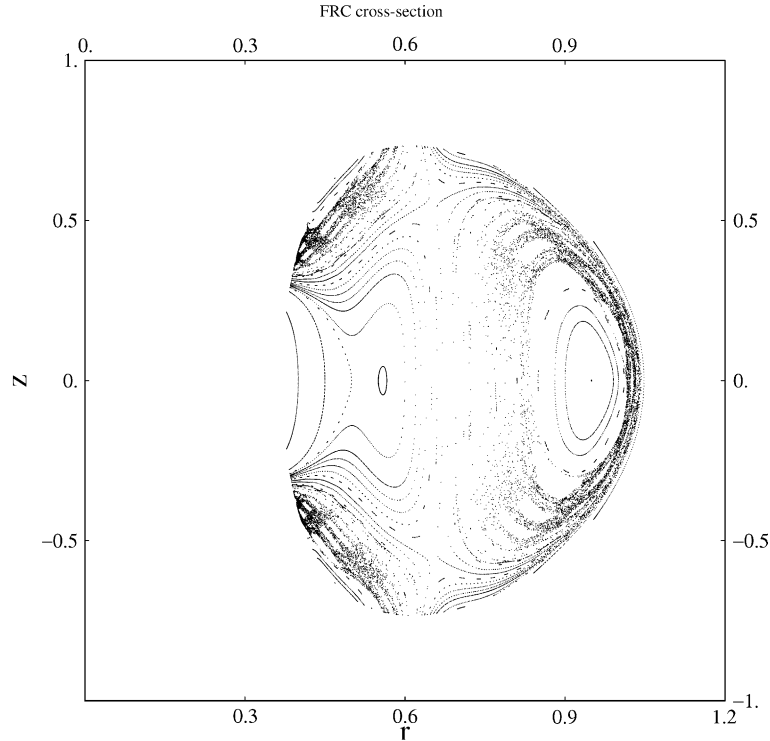


Fig. 6. Cross-section of a trajectory inside the FRC exploring most of the vessel while remaining within its boundaries. Boundary of the vessel occurs at  $\Phi = (1 - r^2 - \beta^2 z^2) = 0$ . Plotted in scaled dimensionless variables,  $E$  denotes total energy.  $E = 0.063$ ,  $\dot{r} = 0$ ,  $P = 0.25$ ,  $\beta = 1$ .

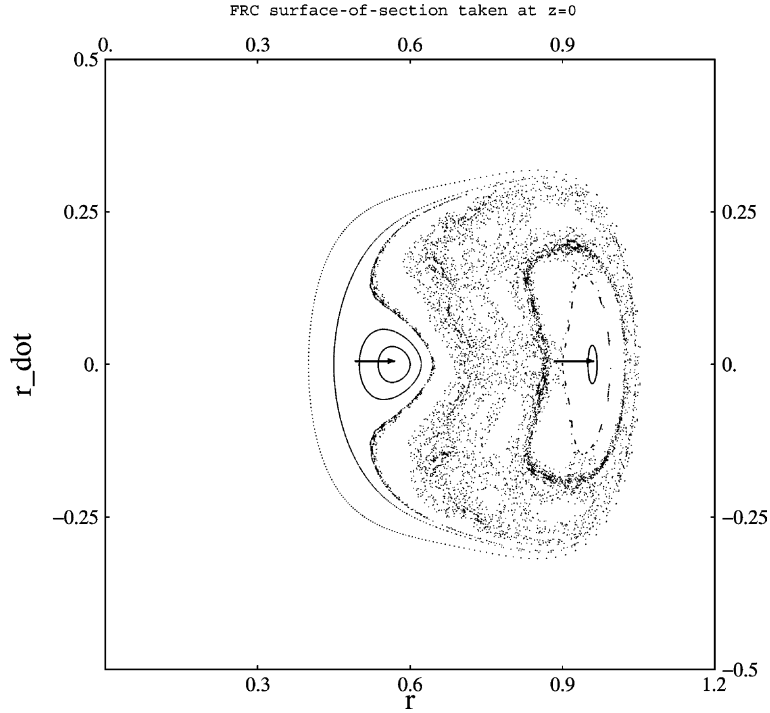


Fig. 7. Overlapping of resonances, leading to an onset of strong chaos (compare with Fig. (8)). The arrows in the figure point to the elliptic centers of the 1:1 resonances. The number of islands increases near the midpoint,  $r_h \approx 0.7$ .  $E = 0.063$ ,  $P = 0.23$ ,  $\beta = 1$ .

From Eq. (46), we can see that (keeping  $q$  constant) the number of islands  $s$  in a single resonance on Poincaré  $p_r$  vs  $r$  plot increases as  $H_r$  decreases, keeping the total energy  $H$  fixed.  $H_r$  is determined by  $A$ , the amplitude of oscillation along  $r$ . Since  $A = r - r_h$ , where  $r$  is taken at  $p_r = 0$ , we expect to get an increasing number of islands corresponding to  $s = \omega_z/\omega_r = 1, 2, 3 \dots$ , as  $A$  becomes smaller, or as we get closer to the midpoint of oscillation at  $r = r_h$ . Figs. 7 and 8 show the increase of islands near the midpoint of oscillation at  $r_h \approx 0.7$ .

As can be seen in Eq. (33),  $F_z$  is multiplied by  $\beta^4$ , so that substituting  $F_z\beta^4$  for  $F$  into Eq. (44), we can see that  $\omega_z$  increases linearly with  $\beta$ , while  $\omega_r$  which depends only on  $F_r$  and  $H_r$  is unaffected. From Eq. (46), a one-to-one resonance occurs whenever

$$\frac{H_z}{H_r} = \frac{F_r}{\beta^4 F_z} \tag{48}$$

It follows that an increase in  $\beta$  has a strong effect on the shift in the location of a one-to-one resonance towards higher amplitudes along  $r$ . Comparison of Figs. 7 and 9 shows this shift towards higher value of  $H_r$  with an increase in  $\beta$ .  $F_r \approx \beta^4 F_z$  for high values of  $\beta$  (around  $\beta \approx 2$ ), corresponding to oblate geometries. Fig. 10 shows  $s/q = 3/2$  resonance around  $H_z = 3H_r$ , close to what we would expect using Eq. (46). Increasing  $\beta$  will lead to a proportional increase of  $s$ , the number of islands, keeping everything else the same.

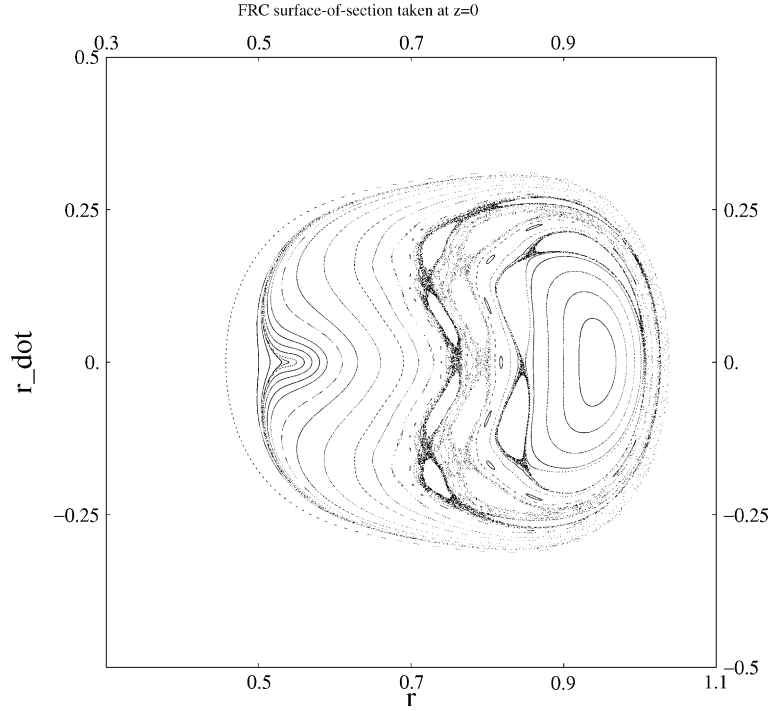


Fig. 8. Set of nonlinear resonances separated by KAM curves. The number of islands increases closer to the midpoint of oscillation,  $r_h$ , where  $r_h \approx 0.7$ .  $E = 0.063$ ,  $P = 0.258$ ,  $\beta = 1$ .

### 3.4. Overlapping of resonances and the onset of strong chaos

The width of an island in a nonlinear resonance depends on the strength of the perturbation,  $\epsilon$  (see Eq. (14)) and  $\alpha$ , the degree of nonlinearity of the unperturbed Hamiltonian  $H_0$ . The nonlinearity  $\alpha$  is defined as [8]

$$\alpha = \frac{J}{\omega} \left| \frac{\partial \omega}{\partial J} \right| \quad (49)$$

In terms of the unperturbed frequency  $\omega$ , the width of an island is given by:

$$\frac{\max \Delta \omega}{\omega} = (\epsilon \alpha)^{\frac{1}{2}} \quad (50)$$

To understand the destruction of KAM surfaces and the occurrence of strong chaos, we introduce Chirikov's parameter  $K_c$ :

$$K_c = \frac{\Delta J}{\delta J} \quad (51)$$

where  $\Delta J$  is the maximum width of the island chain (in action variables) and  $\delta J$  is the distance between neighboring resonances. When  $K_c \ll 1$ , the island chains are clearly separated by KAM

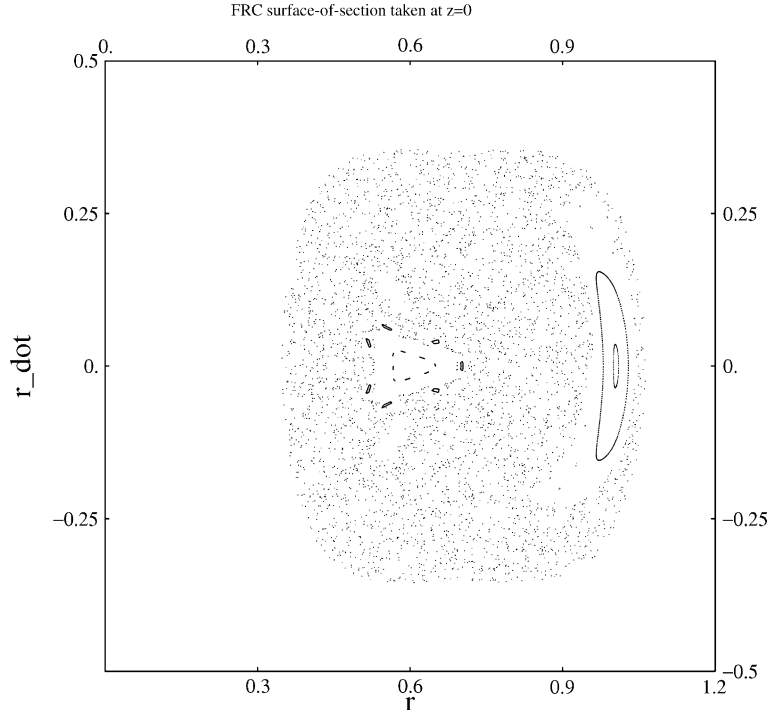


Fig. 9. Outward shift of the outer 1:1 resonance due to an increase in  $\beta$  in a strongly chaotic regime (compare with Fig. (7)).  $E = 0.063$ ,  $P = 0.23$ ,  $\beta = 1.2$ .

curves, between which the trajectories are confined. The resonances begin to overlap when  $K_c > 1$ , leading to an onset of strong chaos, characterized by stochastic behavior over much of the phase-space. Approximating,

$$\Delta\omega = \frac{\partial\omega}{\partial J} \Delta J \tag{52}$$

$$\delta\omega = \frac{\partial\omega}{\partial J} \delta J \tag{53}$$

We can rewrite the criterion for the onset of strong chaos in terms of  $\omega$ :

$$K_c = \frac{\Delta\omega}{\delta\omega} > 1 \tag{54}$$

To estimate the upper limit on  $K_c$ , let us calculate the overlap of the  $q = 1$  resonances. From Eq. (36) the condition for  $s$ -resonance is  $\omega_z = s\omega_r$ , where  $\omega_z$  and  $\omega_r$  are functions of  $\overline{H}_z$  and  $\overline{H}_r$ , respectively. Rewriting the above equation after substituting for  $\omega_r$  from Eq. (44) we get,

$$\omega_z(\overline{H}_z) = s \frac{4}{3a} (F_r \overline{H}_r)^{1/4} \tag{55}$$

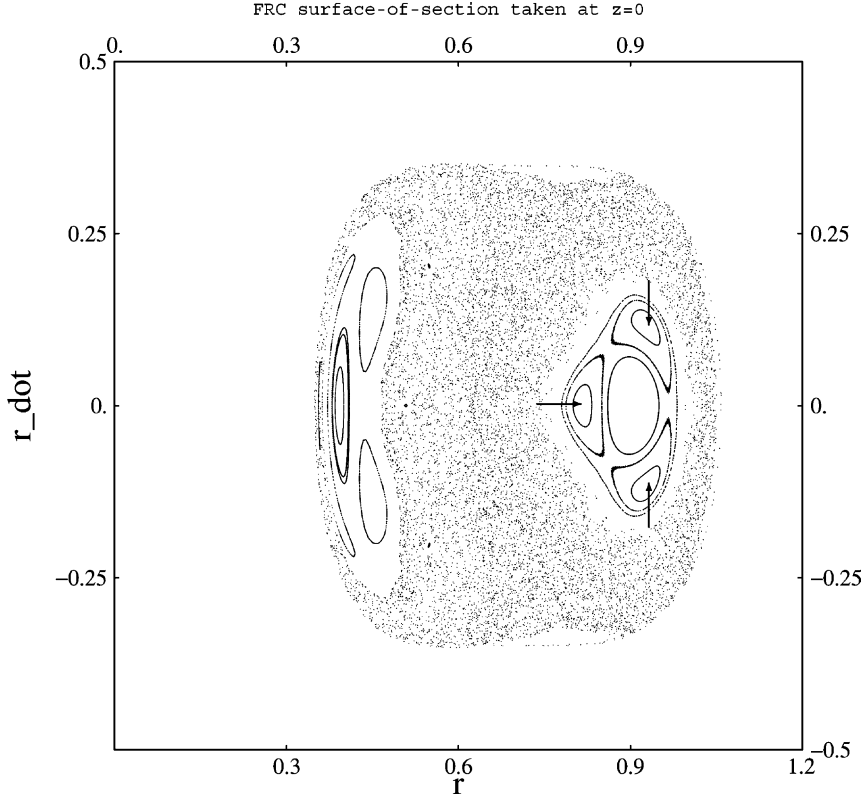


Fig. 10. Resonance at higher  $\beta$ . Arrows point to the elliptic centers of the outer 3:2 resonance.  $E = 0.063$ ,  $P = 0.23$ ,  $\beta = 2$ .

where  $\omega_z(\overline{H}_z)$  indicates that  $\omega_z$  is a function of  $\overline{H}_z$ .  $\overline{H}_r$  and  $\overline{H}_z$  are the energies of the averaged Hamiltonians along  $z$  and  $r$ , respectively, at the  $s$ -resonance. The  $s + 1$  resonance then occurs at  $\overline{H}_z + \delta\overline{H}_z$  and  $\overline{H}_r + \delta\overline{H}_r$ , where  $\delta\overline{H}_r + \delta\overline{H}_z = 0$  to conserve total energy  $H$ .

$$\omega_z(\overline{H}_z + \delta\overline{H}_z) = (s + 1) \frac{4}{3a} (F_r \overline{H}_r)^{1/4} \left( 1 + \frac{\delta\overline{H}_r}{4\overline{H}_r} \right) \quad (56)$$

where we have used the expansion  $(\overline{H}_r + \delta\overline{H}_r)^{1/4} \approx \overline{H}_r^{1/4} (1 + \delta\overline{H}_r/4\overline{H}_r)$ . Expanding Eq. (56), and dropping the smallest term, we get:

$$\omega_z(\overline{H}_z + \delta\overline{H}_z) = s \frac{4}{3a} (F_r \overline{H}_r)^{1/4} \left( 1 + \frac{\delta\overline{H}_r}{4\overline{H}_r} \right) + \frac{4}{3a} (F_r \overline{H}_r)^{1/4} \quad (57)$$

For  $s < 10$  resonances,  $s(\delta\overline{H}_r/4\overline{H}_r) \ll 1$ . Thus Eq. (57) becomes:

$$\omega_z(\overline{H}_z + \delta\overline{H}_z) = s \frac{4}{3a} (F_r \overline{H}_r)^{1/4} + \frac{4}{3a} (F_r \overline{H}_r)^{1/4} \quad (58)$$

Combining Eqs. (58) and (55) and using Eq. (44), we get an expression for  $\delta\omega_z$

$$\delta\omega_z = |\omega_z(\overline{H}_z + \delta\overline{H}_z) - \omega_z(\overline{H}_z)| = \frac{4}{3a} (F_r \overline{H}_r)^{1/4} = \omega_r \quad (59)$$

Using  $\Delta\omega_z = (\epsilon\alpha)^{1/2}\omega_z$  from Eq. (50),  $K_c$  becomes:

$$K_c = \frac{\Delta\omega_z}{\delta\omega_z} = (\epsilon\alpha)^{1/2} \frac{\omega_z}{\omega_r} \quad (60)$$

Thus the criterion for the overlapping of  $q = 1$  resonances is:

$$K_c = (\epsilon\alpha)^{1/2}s > 1 \quad (61)$$

This actually sets the upper limit on  $K_c$ , since other resonances will overlap before the overlap of the  $q = 1$  resonances, resulting in an onset of strong chaos at a lower value of  $K_c$  than that given by Eq. (61). The exact form of the dependence of  $\epsilon$  and  $\alpha$  on  $P$  and  $\beta$  is difficult to obtain, since it would require the expression of the full Hamiltonian given by Eq. (7) in action-angle variables. However, we can find the qualitative relationship between the two sets of variables and thereby explain the overlapping of resonances and the onset of strong chaos observed with variation of  $P$  or  $\beta$ . Multiplying out the terms in Eq. (7), we get:

$$V = \frac{1}{2} \left[ \frac{P^2}{r^2} - P(1 - r^2 - \beta^2 z^2) + r^2(1 - r^2 - \beta^2 z^2)^2 \right] \quad (62)$$

In  $\Delta r$  coordinates (see Eq. (30), where the expansion around  $r_0$  leads to the cancellation of linear terms), the second term in the above equation is quadratic, and the leading contribution from the first term is also quadratic, and therefore linear in the equations of motion. It follows that most of the nonlinearities in the Hamiltonian come from the third  $P$ -independent term, which also contains coupling. It can therefore be concluded that decreasing  $P$  will increase the relative contribution from the nonlinear and coupling terms, and therefore increase both the nonlinearity parameter  $\alpha$  and the coupling  $\epsilon$ . From Eq. (61), an increase in  $\alpha$ ,  $\epsilon$  will result in a greater overlap of resonances and an eventual onset of strong chaos. Fig. 8 shows a set of resonances well bounded by KAM curves, we therefore expect that  $K_c \ll 1$  for this set of parameters. Fig. 7, plotted for a lower value of  $P$ , shows an overlap of resonances. Although some of the island structure is retained and we can still see the location of the different  $s$ -resonances, the destruction of the bounding KAM curves has occurred, resulting in greater region of stochasticity, as compared to Fig. 8. Thus  $K_c > 1$  in Fig. 7, showing a transition to strong chaos.

An increase in  $\beta$  increases the overlap between resonances and therefore chaotic behavior by increasing  $\epsilon$  in Eq. (61). This can be seen by looking at Eq. (10), where the coupling term is the last term in the equation. Since this term is strongly dependent on  $\beta$ , we can expect that an increase in  $\beta$  will also increase the perturbation coefficient  $\epsilon$ . The overlap of resonances and the onset of strong chaos caused by increasing  $\beta$  can be seen in Figs. 7 and 9–11 where the value of  $\beta$  is varied, while  $P$  is kept constant. Thus variation of  $P$  or  $\beta$  effects the degree of stochasticity through  $\alpha$  and  $\epsilon$ , which as shown in Eq. (61), determine the Chirikov parameter  $K_c$ .

### 3.5. Adiabatic limit

Eq. (46) shows a linear dependence of  $s$  on  $\beta$  and a much weaker  $-1/4$  power dependence on  $\bar{H}_r$ . As mentioned before, in the  $z = 0$  subplane, the coordinates separate so that  $\bar{H}_r$  and  $\bar{H}_z$  can be

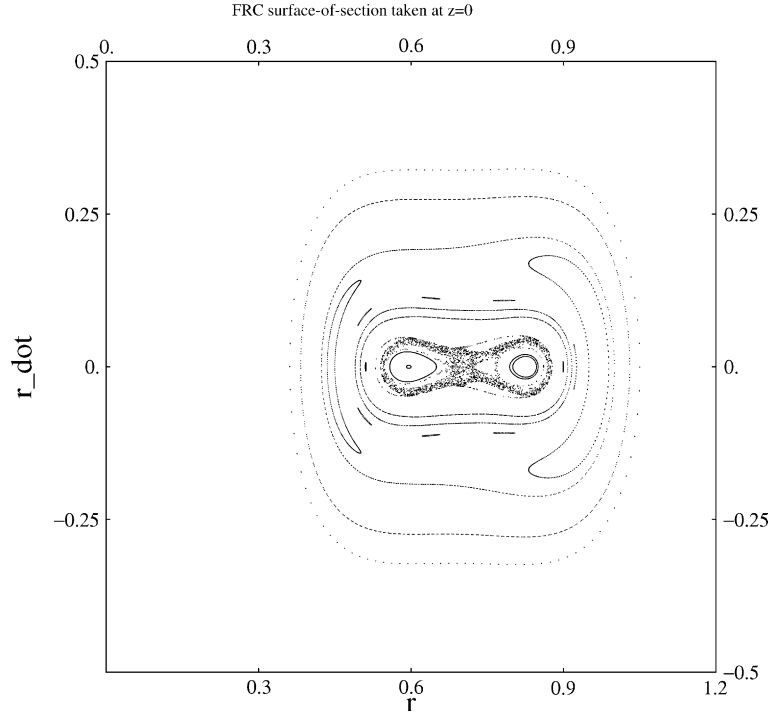


Fig. 11. Shifting of resonances towards the midpoint and the decrease of chaos with decreasing  $\beta$ . Location of 1:1 resonances shifts closer to the midpoint of oscillation,  $r_h \approx 0.7$ , as  $\beta$  is lowered.  $E = 0.063$ ,  $P = 0.23$ ,  $\beta = 1/2$ .

replaced by  $H_r$  and  $H_z$ , respectively (see Eq. (45)), as long as the motion is not too affected by the resonance. Using Eq. (46), we expect a decrease in  $\beta$  to strongly shift the location of a one-to-one resonance towards smaller values of  $H_r$  or closer to the midpoint of oscillation at  $r = r_h$ , in the  $z = 0$  plane. Fig. 11 shows this for  $\beta = 1/2$ . There is only a thin layer of stochasticity close to the separatrix, due to the very low values of  $H_r$  (or amplitude of oscillation  $A$ ) where the resonance occurs.

As the value of  $\beta$  is further decreased, the quadratic terms in Eq. (28) can no longer be neglected, leading to behavior different than what would be expected based on previous analysis (Figs. 12 and 13). To understand the motion at  $\beta^2 \ll 1$ , let us turn to Eqs. (10) and (11). It can be seen that there is a separation of time scales between  $r$  and  $z$  motion in the limit of small  $\beta$ . Since the motion along  $r$  is much faster than the motion along  $z$ ,  $J_r$  is a conserved adiabatic invariant, except during the crossing of the separatrix [17,19,20]. At the approach to the separatrix the frequency,  $\omega_r$ , slows down leading to a breakdown of  $\omega_r \gg \omega_z$  condition required for the adiabatic invariance of  $J_r$ . The change in  $J_r$  during each crossing is  $\sim \beta \ln(\beta)$  [21]. This leads to mostly chaotic orbits inside and close to the separatrix as shown in Fig. 13.

To avoid the crossing of the separatrix that occurs during a transition between cyclotron and figure-8 orbits, the action  $J_r$  has to be high enough so that the ion executes a figure-8 orbit with  $\omega_r \gg \omega_z$  when it passes  $z = 0$  subplane. To ensure the adiabatic invariance of  $J_r$ , we can find a lower limit on its value by choosing  $H_{r_{\min}} = (1 + \delta_c)V(r_h, 0)$ , where  $\delta_c \ll 1$  [22], calculating the

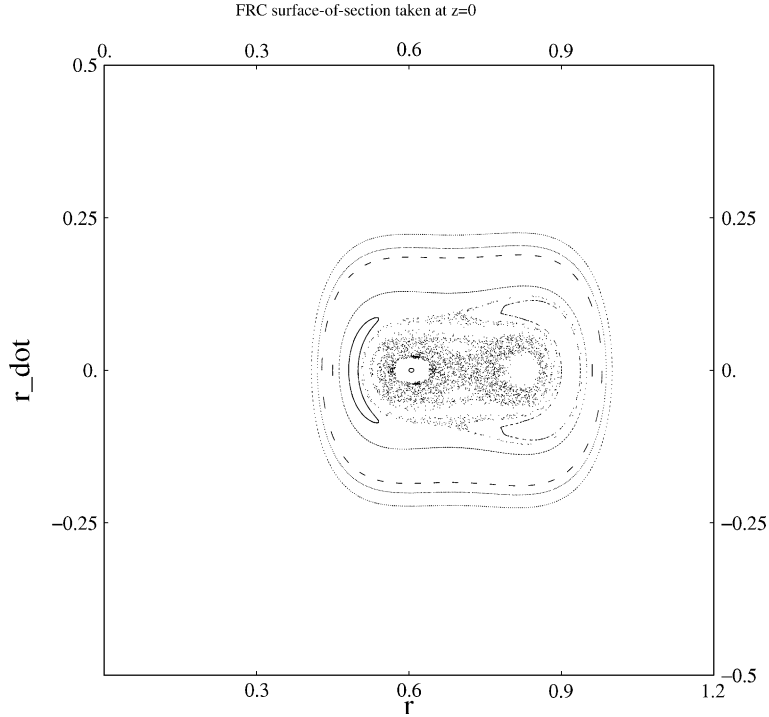


Fig. 12. Chaos at lower values of  $\beta$  where the quartic approximation fails.  $E = 0.063$ ,  $P = 0.23$ ,  $\beta = 0.3$ .

resultant  $p_r$  as a function of  $r$ , and substituting it into the integral in Eq. (15). The condition for integrable orbits becomes:

$$J_r > \frac{1}{2\pi} \oint \left\{ (1 + \delta_c)V(r_h, 0) - \left[ \frac{P}{r} - r(1 - r^2) \right]^2 \right\}^{\frac{1}{2}} dr \quad (63)$$

The above integral is the action of the ion in the  $z = 0$  subspace when  $H_r$  is just high enough for the ion to pass over the energy barrier at some finite speed and execute figure-8 orbits.  $r_h^2 = K_1$  is the location of the top of the barrier evaluated at  $z = 0$  (Eq. (26)). The factor of  $(1 + \delta_c)$  insures that the motion is not too close to the phase-space separatrix. Since  $J_r$  is conserved for integrable orbits, Eq. (63) provides a threshold above which orbits are integrable.

Fig. 14 shows the area inside the phase-space separatrix,  $J_{rs}$ , in the  $z = 0$  cross-section as a function of  $P$ . All orbits passing through the  $z = 0$  plane with  $J < J_{rs}$ , will cross the separatrix as the area inside shrinks with motion towards higher  $|z|$  values. This leads to mostly chaotic orbits inside and close to the separatrix as shown in Fig. 13. The shrinking of the area inside the phase-space separatrix is due to the drop of the potential barrier along  $r$  as the ion moves towards higher absolute values of  $z$  (see Fig. 3). Thus most of the cyclotron orbits in the low  $\beta$  limit should be stochastic due to a repeated violation of  $J_r$ . Above a critical value of  $P = P_c$ , all cyclotron orbits disappear and only betatron orbits exist, we would therefore expect mostly integrable orbits.

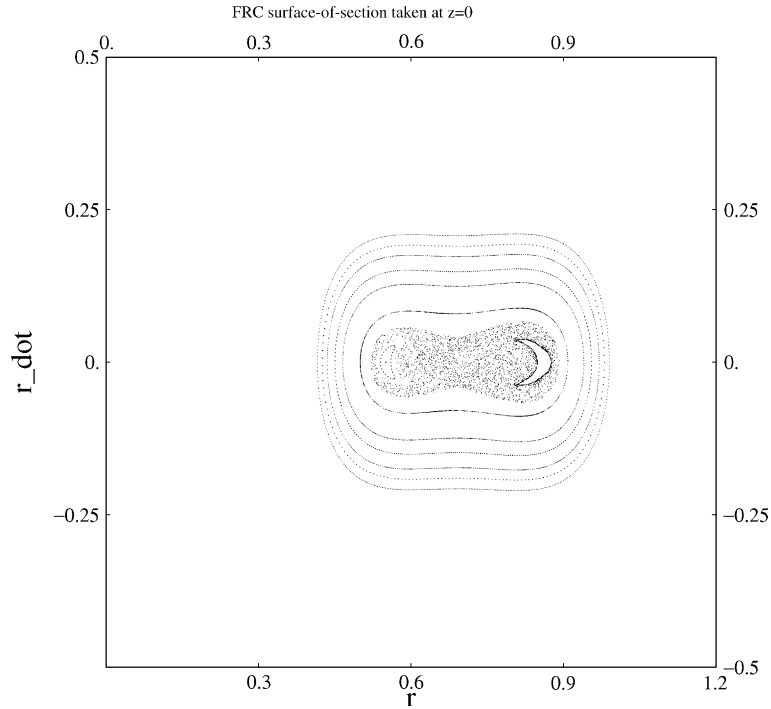


Fig. 13. The adiabatic limit occurring for small  $\beta$  values. Most orbits inside and close to the separatrix are chaotic.  $E = 0.063$ ,  $P = 0.23$ ,  $\beta = 0.2$ .

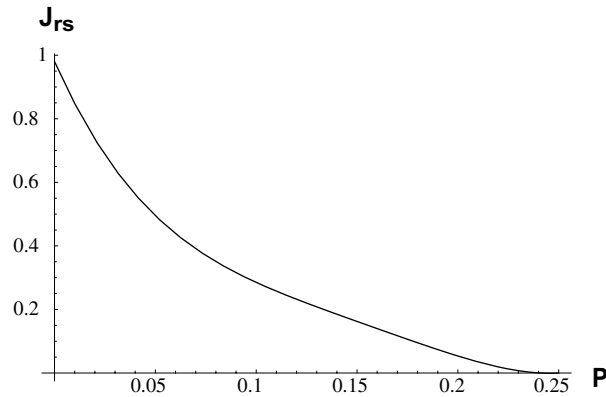


Fig. 14. The area inside the phase-space separatrix,  $J_{rs}$ , in the  $z = 0$  cross-section as a function of  $P$ . Orbits lying below the curve are chaotic.

#### 4. Universal resonance and intrinsic degeneracy

At higher values of  $P$ , the quadratic terms become more important for ions confined to the FRC. This can be seen in Fig. 5 where the quadratic coefficient crosses zero below  $P_c$  (if the

amplitude terms are taken into account) and continues to increase as  $P$  increases. It follows that at higher values of  $P$  (about  $P > 6P_c/5$  for the energies used), the unperturbed Hamiltonian can be expressed as uncoupled simple harmonic oscillators. Expanding the Hamiltonian in Eq. (7) around  $r_0 = K_1^{1/2}$ , so that  $\Delta r = r - r_0$ , and grouping all nonquadratic terms under the perturbation term,  $H_1$ , we get

$$H = \frac{1}{2}p_r^2 + \frac{1}{2}p_z^2 + \frac{1}{2}D_{r0}\Delta r^2 + \frac{1}{2}\beta^2 D_{z0}z^2 + \epsilon H_1(\Delta r, z) \quad (64)$$

where  $D_{r0}$  and  $\beta^2 D_{z0}$  are the coefficients of the quadratic coordinate terms in the expansion of the Hamiltonian

$$D_{r0} = 1 + 2P - 12K_1 + 15K_1^2 + \frac{3P^2}{K_1^2} \quad (65)$$

$$\beta^2 D_{z0} = \beta^2(2P - 2K_1 + 2K_1^2) \quad (66)$$

with  $K_1$  is given by Eq. (27).

In action-angle variables the coordinates of a simple harmonic oscillator are given by [7]

$$\Delta r = \left( \frac{2J_r}{R_r} \right)^{1/2} \sin \theta_r \quad (67)$$

$$p_r = (2J_r R_r)^{1/2} \cos \theta_r \quad (68)$$

$$z = \left( \frac{2J_z}{R_z} \right)^{1/2} \sin \theta_z \quad (69)$$

$$p_z = (2J_z R_z)^{1/2} \cos \theta_z \quad (70)$$

where  $R_r = D_{r0}^{1/2}$  and  $R_z = \beta D_{z0}^{1/2}$ . Substituting action-angle variables from Eqs. (67)–(70) into the expanded Hamiltonian in Eq. (64), we get

$$H = \omega_r J_r + \omega_z J_z + \epsilon H_1(\vec{J}, \vec{\theta}) \quad (71)$$

where  $\omega_r$  and  $\omega_z$  are the frequencies of the unperturbed quadratic Hamiltonian,

$$\omega_r = D_{r0}^{1/2} \quad \omega_z = \beta D_{z0}^{1/2} \quad (72)$$

In action-angle variables,  $H_1$  can be expanded as:

$$H_1 = \sum_{l,m=-\infty}^{\infty} H_{l,m}(\vec{J}) \exp(i\vec{n} \cdot \vec{\theta}) \quad (73)$$

In the absence of resonances, Eq. (71) is integrable and the conserved invariants, close to  $J_r$  and  $J_z$ , can be found by applying standard perturbation theory and expanding in the same way as for a one-dimensional system. The terms in  $H_1$  can be easily found by expanding the Hamiltonian around  $r_0$ , as was done in Eq. (64), and substituting action-angle variables, given by Eqs. (67)–(70). The exact expression for  $H_{1,-1}$  will be given below, relating to a discussion of a 1:1 universal resonance.

A resonance will occur whenever the conditions of Eq. (24) are satisfied, with  $\omega_r$  and  $\omega_z$  given by Eq. (72). The width of the island in a resonance for a Hamiltonian given by Eq. (71) should be large, due to the intrinsic degeneracy, since the unperturbed frequencies,  $\omega_r$  and  $\omega_z$ , are constant, thereby leading to a universal resonance. In this case, transforming to a rotating frame:

$$J_r = s\hat{J}_1; \quad J_z = \hat{J}_2 - q\hat{J}_1; \quad \hat{\theta}_1 = s\theta_r - q\theta_z; \quad \hat{\theta}_2 = \theta_z \quad (74)$$

the unperturbed Hamiltonian in Eq. (71) is a function of  $qJ_r + sJ_z$  (where  $\omega_z/\omega_r = s/q$ ) or in rotating coordinates:

$$\hat{H}_0 = \hat{H}_0(\hat{J}_2) \quad (75)$$

that is,  $H_0$  is independent of  $\hat{J}_1$ .

Following Lichtenberg and Lieberman [7], in the presence of a resonance in an intrinsically degenerate system (where  $\omega_r$  and  $\omega_z$  are constant), the perturbation to the Hamiltonian is

$$\Delta\bar{H} = \frac{1}{2}G(\Delta\hat{J}_1)^2 + \frac{1}{2}F(\Delta\hat{\theta}_1)^2 \quad (76)$$

where the bar above  $\Delta H$  signifies that averaging over the fast variable  $\hat{\theta}_2$  has been performed.  $G$  is a nonlinearity parameter proportional to  $\epsilon$

$$G = \epsilon \frac{\partial^2 H_{0,0}}{\partial \hat{J}_{10}^2} + \epsilon \frac{\partial^2 H_{s,-q}}{\partial \hat{J}_{10}^2} \quad (77)$$

$F$  is also proportional to  $\epsilon$ ,

$$F = -2\epsilon H_{s,-q} \quad (78)$$

Eq. (76) was obtained by transforming to rotating coordinates  $\vec{\hat{J}}$  and  $\vec{\hat{\theta}}$ , where  $\hat{\theta}_1$  and  $\hat{\theta}_2$  are the slow and fast variables, respectively. Then averaging over the fast variable  $\hat{\theta}_2$ , and expanding the highest order resonant terms around the elliptic point of the resonance at  $\hat{J}_1 = \hat{J}_{10}$  and  $\hat{\theta}_1 = 0$ . Since the nonlinearity parameter  $G$  in Eq. (76) is small (of order  $\epsilon$ ), we can expect maximum excursion in  $\Delta\hat{J}_1$  to be large. This explains why intrinsically degenerate systems have large resonances [7].

The equations given above can be used for analytic study of specific resonances that occur at different values of  $\beta$ . Eqs. (65) and (66) determine the range of values of  $P$  and  $\beta$  for which different resonances occur. Fig. 15 shows  $D_{r,0}$  and  $\beta^2 D_{z,0}$  for  $\beta = 2$  plotted as a function of  $P$ . It can be seen that the two coefficients are close for a range of values of  $P$ , creating a universal one-to-one resonance. To estimate  $\Delta\bar{H}$  and  $\Delta\hat{J}_1$ , (or  $\Delta J_r$ ), for the case of the one-to-one resonance, we express  $\epsilon H_1$  in action-angle variables and find  $G$  and  $F = -2\epsilon H_{1,-1}$ , in accordance with Eqs. (77) and (78). Changing back to  $(J_r, J_z)$  variables, keeping only the terms of lowest power in  $\vec{J}$ , a valid approximation for ions confined inside the FRC, we get

$$G \approx \frac{1}{R_r^2} \left( 6K_1 + \frac{15P^2}{2K_1^3} \right) \quad (79)$$

$$F \approx \frac{1}{2R_r^2} (6K_1 - 1) J_r J_z \quad (80)$$

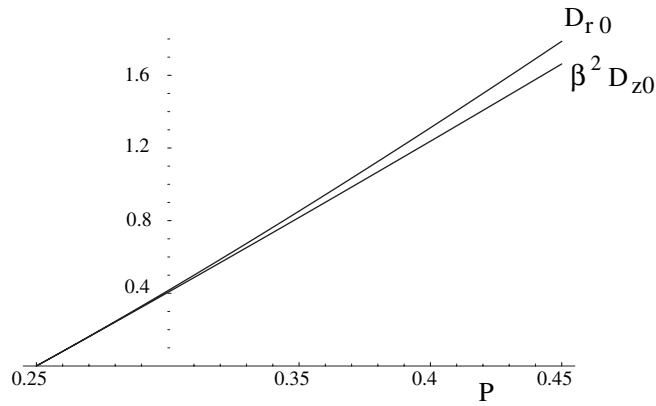


Fig. 15. Quadratic coefficients of  $H_0$  as a function of  $P$  for the case of a universal 1:1 resonance at  $\beta = 2$ . Below  $P = 0.25$  fourth power terms dominate.

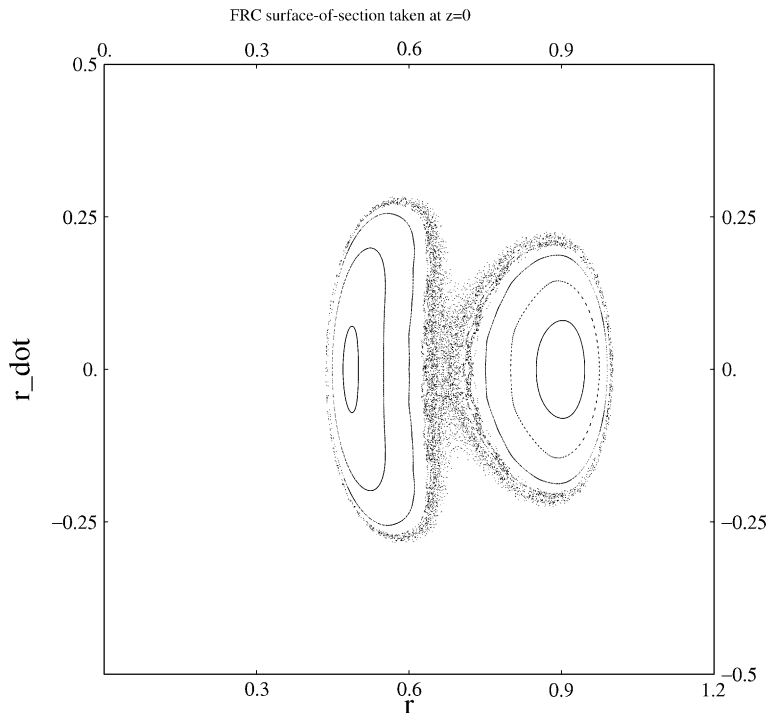


Fig. 16. Universal 1:1 resonance occurring as a result of intrinsic degeneracy, onset at higher  $P$  values.  $E = 0.063$ ,  $P = 0.3$ ,  $\beta = 2$ .

To compare the magnitudes of  $G$  and  $F$ , keep in mind that  $K_1^{1/2}$  is the midpoint of oscillation in the  $z = 0$  subplane, so that for the ions oscillating inside the FRC:  $K_1 \sim 1/2$ . In dimensionless variables adopted throughout this paper, the magnetic field separatrix (to be distinguished from

the phase-space separatrix) at  $z = 0$  is located at  $r = 1$ . From Eq. (76) the maximum fluctuation in energy for a one-to-one resonance is given by,

$$\Delta\bar{H} \approx (\pi^2/2)F \quad (81)$$

with  $F$  given by Eq. (80). The maximum change in  $J_r$  for a one-to-one resonance can be estimated by setting  $J_r = \hat{J}_1$  (see Eq. (74)) and using Eq. (76) to obtain:

$$\left(\frac{G}{F}\right)^{1/2} \left(\frac{\Delta J_{r\max}}{\pi}\right) = O(1) \quad (82)$$

Substituting Eqs. (79) and (80) into Eq. (82), using  $J_r \sim J_z$ , we get,

$$\frac{\Delta J_{r\max}}{J_r} \sim O(1) \quad (83)$$

indicating that the changes in action in a universal resonance are large. Fig. 16 shows a universal one-to-one resonance that occurs at  $\beta = 2$  for a range of values of  $P$ . The fluctuations caused by the resonance are large due to the intrinsic degeneracy of the system in this regime.

## 5. Conclusion

After reducing the three-dimensional Hamiltonian of an ion inside the FRC to that of a particle moving in a two-dimensional potential, possible types of ion orbits for positive azimuthal angular momentum  $P$  were derived. Then the effects of variation in  $P$  and inverse elongation  $\beta$  were investigated. A method of averaging was used to study the structure of nonlinear resonances. It turns out that at intermediate values of  $P$ , the fourth order terms in the averaged Hamiltonian predominate. In this case, the unperturbed frequencies  $\omega_r$  and  $\omega_z$  can be derived as a function of the averaged Hamiltonians  $\hat{H}_r$  and  $\hat{H}_z$ , respectively. Based on these frequencies, the occurrence of various  $s$  resonances, where  $s = \omega_z/\omega_r$ , can be calculated. It was found that increasing  $\beta$  shifts the location of the resonance outward towards higher values of  $\hat{H}_r$ . High values of  $\beta$  are found to produce high  $s$  resonances. The structure of the resonances was such that higher  $s$  resonances were found closer to the midpoint of oscillation along  $r$ . The dependence of Chirikov's island overlap parameter,  $K_c$ , on the magnitude of the perturbation  $\epsilon$  and nonlinearity  $\alpha$  was derived and the qualitative relationship between  $\epsilon$ ,  $\alpha$  and  $\beta$ ,  $P$  discussed. It was found that lowering  $P$  or increasing  $\beta$  cause an increase in  $\epsilon$  and  $\alpha$ , leading to a greater overlap of resonances and the eventual onset of strong chaos. In the adiabatic regime, occurring for large elongations (small  $\beta$ ), orbits outside the phase-space separatrix, in the  $z = 0$  subplane were shown to be integrable, while the majority of orbits inside the phase-space separatrix were not. This is due to separation of time scales  $\omega_r \gg \omega_z$  that occurs for orbits which do not cross the phase-space separatrix.

Next, the universal resonance resulting from intrinsic degeneracy of the Hamiltonian at higher values of  $P$  was investigated. Under these circumstances, the unperturbed frequencies are constant, and the Hamiltonian can be expressed in action-angle variables of a simple harmonic oscillator. The width of the resonances can then be derived from the perturbation term  $H_1$ . For high  $P$  case, most of the orbits are integrable, except in case of a resonance when  $\omega_z/\omega_r = q/s$ , where  $q$  and  $s$  are integers. After deriving an expression for unperturbed frequencies in this

degenerate regime, a universal one-to-one resonance was found analytically and numerically at  $\beta = 2$  for a range of values of  $P$ . The width of this resonance was estimated and the fluctuations in action found to be large (of order one), as would be expected for a degenerate case.

### Acknowledgements

This work was supported, in part, by US Department of Energy contract no. DE-FG02-92ER54184.

### References

- [1] Tuszewski M. Review paper: field reversed configurations. *Nucl Fusion* 1988;28:2033–92.
- [2] Tuszewski M, Taggart DP, Chrien R, Rej DJ, Siemon RE, Wright BL. Axial dynamics in field-reversed theta pinches. *Phys Fluids B* 1991;3:2856–70.
- [3] Friedberg JP, Haney SW. Variational methods for studying tokamak stability in the presence of a thin resistive wall. *Phys Fluids B* 1989;1:1637–45.
- [4] Finn JM, Sudan RN. Review paper: field reversed configurations with a component of energetic particles. *Nucl Fusion* 1982;22:1443–518.
- [5] Glasser AH, Cohen SA. Ion and electron acceleration in the field-reversed configuration with odd-parity rotating magnetic field. *Phys Plasmas* 2002;9:2093–102.
- [6] Sagdeev RZ, Usikov DA, Zaslavsky GM. *Nonlinear physics*. Philadelphia: Harwood Academic Publishers; 1992.
- [7] Lichtenberg AJ, Leiberman MA. *Regular and chaotic dynamics*. New York: Springer-Verlag; 1992.
- [8] Zaslavsky GM. *Physics of chaos in Hamiltonian systems*. London: Imperial College Press; 1998.
- [9] Luo ACJ, Han RPS. Analytical predictions of chaos in a non-linear rod. *J Sound Vibr* 1999;227(3):523–44.
- [10] Luo ACJ, Han RPS. The dynamics of stochastic and resonant layers in a periodically driven pendulum. *Chaos, Solitons & Fractals* 1999;11:2349–59.
- [11] Zaslavsky GM, Filonenko NN. Stochastic instability of trapped particles and conditions of application of the quasi-linear approximation. *Sov Phys JETP* 1968;27:251–7.
- [12] Luo ACJ. Resonant layers in a parametrically excited pendulum. *Int J Bifurcat Chaos* 2002;12(2):409–19.
- [13] Goldstein H. *Classical mechanics*. Reading: Addison-Wesley; 1980.
- [14] Solov'ev LS. The theory of hydromagnetic stability of toroidal plasma configurations. *Sov Phys JETP* 1968;26:400–7.
- [15] Hugrass W, Turley M. The orbits of electrons and ions in the fields of the rotamak. *J Plasma Phys* 1987;37:1–13.
- [16] Wang MY, Miley GH. Particle orbits in field-reversed mirrors. *Nucl Fusion* 1979;19:39–49.
- [17] Landsman AS, Cohen SA, Glasser AH. Regular and stochastic orbits of ions in a highly prolate field-reversed configuration. *Phys Plasmas* 2004;11:247.
- [18] Cohen SA, Glasser AH. Ion heating in the field-reversed configuration by rotating magnetic fields near the ion-cyclotron resonance. *Phys Rev Lett* 2000;85:5114–7.
- [19] Kim J-S, Cary JR. Charged particle motion near a linear magnetic null. *Phys Fluids* 1983;26:2167.
- [20] Neishtadt AI. Change of an adiabatic invariant at a separatrix. *Sov J Plasma Phys* 1986;12:568–73.
- [21] Cary JR, Escande DF, Tennyson JL. Adiabatic invariant changes due to separatrix crossing. *Phys Rev A* 1986;34:4256–75.
- [22] Neishtadt AI. Stable periodic motions in the problem of passage through separatrix. *Chaos* 1997;7:2–11.